Faraday Discussions

Cite this: *Faraday Discuss.*, 2016, **193**, 41

PAPER

View Article Online
View Journal | View Issue

Single-molecule electrochemistry in nanochannels: probing the time of first passage†

Shuo Kang, Ab F. Nieuwenhuis, Klaus Mathwig,‡ Dileep Mampallil,§ Zinaida A. Kostiuchenko and Serge G. Lemay*

Received 11th April 2016, Accepted 19th April 2016
DOI: 10.1039/c6fd00075d

The diffusive mass transport of individual redox molecules was probed experimentally in microfabricated nanogap electrodes. The residence times for molecules inside a well-defined detection volume were extracted and the resulting distribution was compared with quantitative analytical predictions from random-walk theory for the time of first passage. The results suggest that a small number of strongly adsorbing sites strongly influence mass transport at trace analyte levels.

Introduction

The ability to address and probe individual molecules has led to significant new insights on molecular transport and internal dynamics in fields ranging from molecular electronics to biophysics.[1,2] It is thus of considerable interest to extend the range of single-molecule analysis methods to other transduction mechanisms such as electrochemistry. While single-molecule detection by electrochemical means has indeed been reported,[3–7] efforts so far have focused almost exclusively on demonstrating the basic ability to resolve single molecules and have not allowed for deeper analysis. This is largely due to the experimental challenge inherent in measuring the extremely small signal levels associated with single-molecule faradaic processes.

Here we demonstrate for the first time the ability to statistically analyse the diffusive dynamics of individual molecules using an electrochemical method. We

MESA+ Institute for Nanotechnology, University of Twente, PO Box 217, 7500 AE Enschede, The Netherlands. E-mail: S.G.Lemay@utwente.nl

† In response to comments raised during the discussion of this manuscript, Eqn (2) and Fig. (3) of the manuscript have been altered from the preprint version. Eq. (2) was rewritten in its exact form instead of the earlier, approximate form and an error in the normalization of the theoretical curves in Fig. (3) was corrected.

‡ Present address: Groningen Research Institute of Pharmacy, University of Groningen, P.O. Box 196, 9700 AD Groningen, The Netherlands.

§ Present address: Indian Institute of Science Education & Research Tirupati, Mangalam P. O. Tirupati 517 507, India.

focus on the distribution of residence times for molecules randomly entering and leaving a nanofluidic cavity, an inherently single-molecule property. The residence time corresponds to a well-studied quantity in stochastic systems, the so-called first-passage time,[8] which appears in diverse fields including ecology,[9] biophysics,[10–12] finance,[13] diffusion-controlled chemical reactions,[14] *etc.*,[15] and which permits a quantitative comparison of the measurements with theory.

Experimental methods

Redox cycling in nanogap transducers offers the possibility to record extensive, high-quality single-molecule amperometric data.[6] The nanogap device is sketched in Fig. 1a. It consists of two electrodes with a length $L = 50$ μm and a width of 4 or 5 μm that are separated by a solution-filled gap of 40 nm. The device was microfabricated using optical lithography, as described earlier.[6] In brief, a stack of metal layers (Pt/Cr/Pt) was first deposited and patterned on a 4-inch Si wafer,

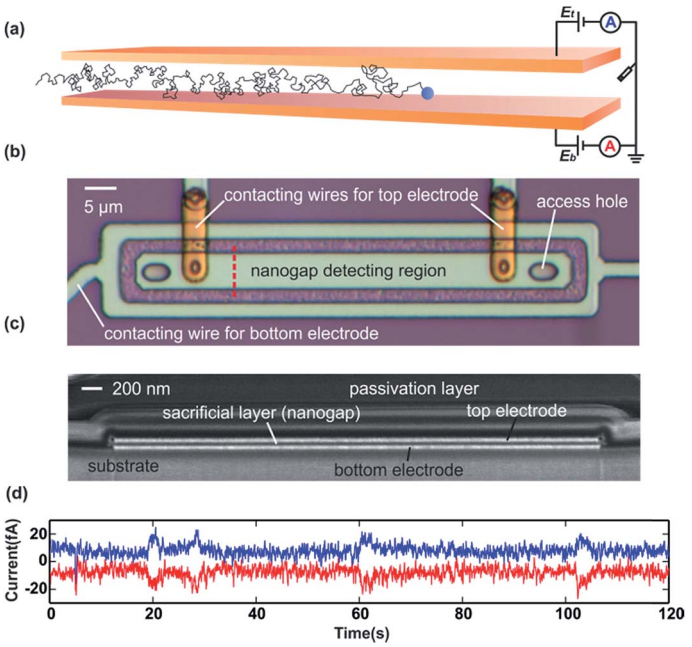

Fig. 1 (a) Schematic illustration of a nanogap device. (b) Optical microscope image (top view) of a device. The cyan rectangle in the center corresponds to the top electrode, below which lies the detection region. The remaining structures serve as electrical interconnects to the top and bottom electrodes (yellow and cyan lines, respectively). (c) Scanning electron microscopy image of the cross section of a device from a 52° viewing angle. To make this image the device was cut open using a focused ion beam along the line indicated by the dashed red line in (b). (d) Current-time traces simultaneously measured at the top (blue) and bottom (red) electrodes (width 5 μm) under redox-cycling conditions (10 pM FcTMABr in 0.1 M KCl aqueous solution, $E_t = 0.5$ V and $E_b = 0.35$ V). The traces have been offset vertically for clarity. Several single-molecule events with duration >1 second appear as abrupt changes in the currents compared to the baseline. These transients have opposite signs at the two electrodes as a result of redox cycling (oxidation and reduction at the top and bottom electrode, respectively).

 This journal is © The Royal Society of Chemistry 2016

followed by ion-beam etching (IBE) and subsequent wet etching to define the active nanogap detecting region. A final metal layer sandwiched between two passivation layers was then deposited and patterned to provide electrical connections to the top electrode. Finally, access holes for liquid were created by etching through the passivation and top electrode. The sacrificial layer was wet-etched *via* the access holes immediately before use, releasing the 40 nm high nanochannel. An optical microscope image of a complete device and a scanning electron microscope image of the nanogap cross section are shown in Fig. 1b and c, respectively.

The measurements were performed by interfacing the device with an external reservoir containing an aqueous solution with a concentration $C = 10$ pM of redox species and 0.1 M KCl as supporting electrolyte. The average number of analyte molecules in solution in the detection region was then $\langle N \rangle = CVN_A = 0.05$ for a device with a width of 4 μm, where $V = 8 \times 10^{-18}$ m^3 is the volume of the nanogap region and N_A is Avogadro's number. For a 5 μm wide device, $\langle N \rangle = 0.06$ under the same conditions. For such low occupancy, the fraction of the time that the device is occupied by two or more molecules at the same time is low (<0.2%) based on Poisson statistics.

For single-molecule experiments, the bottom and top electrodes were biased at reducing and oxidizing potentials, respectively. Under these redox-cycling conditions, each chemically reversible redox molecule present in the nanogap is repeatedly oxidized and reduced as it undergoes Brownian motion, generating faradaic currents of opposite polarity at the two electrodes. These reduction and oxidation currents were measured simultaneously; each time that a molecule randomly entered and subsequently exited the nanochannel, current steps with magnitudes of the order 10^{-14} A and opposite signs were observed in the measured currents. This is illustrated in Fig. 1d, which shows a time trace with four distinctly recognizable single-molecule events with durations of the order of a few seconds.

In order to achieve sufficient sensitivity to detect these extremely low currents, current-to-voltage converters with 10^{12} V A^{-1} trans-impedance gain and a response time of 350 ms (10–90% rise time) were employed (FEMTO DDPCA-300).[16] Such a slow response is essentially unavoidable due to the inverse relationship between gain and measurement bandwidth in high-gain amplifiers. Consequently, and as discussed further below, only events lasting longer than ~450 ms could be reliably resolved.

Results and discussion

Numerical simulations

To ascertain the feasibility of identifying single-molecule events from the experimental data and accurately determining their durations, we performed random walk simulations of individual molecular trajectories. We have previously shown that, due to the devices' highly anisotropic geometry, Brownian motion in nanogap transducers such as the ones employed here can be modelled as a discrete 1D random walk.[17] At each time step a diffusive molecule makes a random jump to the left or right with a step size $\Delta x = L/a$, where L is the length of the device and $a - 1$ ($\gg 1$) is the number of spatial grid points in the simulation. In order to ensure consistency with the macroscopic diffusion coefficient,

D, the size of each time step is taken as $\Delta t = \Delta x^2/2D$. We emphasize that this simple algorithm is sufficient to provide an accurate description of Brownian motion on length and time scales significantly larger than Δx and Δt, respectively, even when Δx and Δt are themselves much larger than the microscopic scales associated with individual molecular collisions in the liquid. In the simulation, the two grid points at the edges of the simulated domain correspond to positions adjacent to the two access holes of the device. Molecules that hop outside the simulated domain are considered to have exited the device through these holes, while molecules diffusing into the device are represented by a probability p that a new molecule appears at either end of the simulated domain at each time step. In the steady state, the average rates of entry and egress are equal and the average number of molecules inside the device, $\langle N \rangle$, is constant; the value of $\langle N \rangle$ can be tuned by adjusting the value of p. Interactions between molecules are neglected.

Fig. 2a shows a typical trace of the device occupancy *versus* time for an average occupancy $\langle N \rangle = 0.1$. Most events are very short, with only a minority of events having durations of the order of seconds. To simulate the role of the measurement electronics, the occupancy was first converted to a current as $I(t) = N(t)i_p$, where i_p is the redox-cycling current per molecule. White noise was then added and the resulting traces were convolved with a first-order impulse response (a simple exponential) with a time constant of $\tau = 350$ ms that corresponds to the experimental apparatus. The result for the trace in Fig. 2a is shown in Fig. 2b. Events with a duration of order 1 s reach (or even temporarily exceed, because of noise) the full single-molecule current, i_p. Such events exhibit a trapezoid shape, with a full width at half-maximum that agrees within $\pm 10\%$ with the duration of the underlying event in Fig. 2a. Longer events (not shown) instead exhibit a well-defined plateau, while events with durations of order $\tau = 450$ ms or shorter contribute to the apparent noise in the current but cannot be reliably identified. Occasionally two long events are juxtaposed and cannot be distinguished, as illustrated in Fig. 2 around 17 s. However, at this low average occupancy such occurrences are rare, as are occurrences of two long events overlapping for a short time. Multiple occupancy thus has minimal impact on the overall statistics. Taken together, these simulation

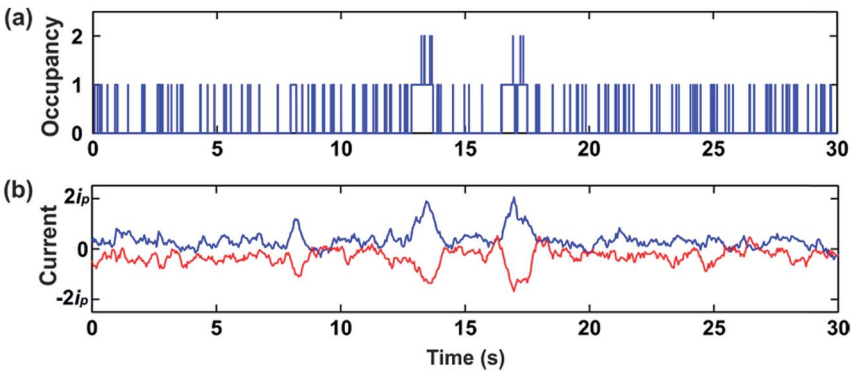

Fig. 2 (a) Simulated occupancy–time trace for an average occupancy $\langle N \rangle = 0.1$. (b) Corresponding simulated current–time trace including additive Gaussian noise (3 fA_{rms}) and filtered to account for the influence of the measurement electronics. The current per molecule, i_p, is assumed to be 15 fA.

 This journal is © The Royal Society of Chemistry 2016

results suggest that it is feasible to accurately identify single-molecule events longer than $\tau = 450$ ms and to determine their duration.

Single-molecule measurements

Extensive current–time traces were recorded with aqueous solutions of 10 pM ferrocenedimethanol ($1Fc(MeOH)_2$, $E^{\circ\prime} = 0.25$ V) and 10 pM ferricyanide $[Fe(CN)_6]^{3-}$, $E^{\circ\prime} = 0.23$ V) in 0.1 M KCl under redox cycling conditions ($E_t = 0.3$ V, $E_b = 0.2$ V for $Fc(MeOH)_2$ and $E_t = 0.3$ V, $E_b = 0.15$ V for $[Fe(CN)_6]^{3-}$) in 4 μm and 5 μm wide devices, respectively, as shown in Fig. 3a and c. Single-molecule events were identified and their durations were extracted from these amperometric data. Fig. 3b and d show the histograms of event durations extracted from 26 min and 20 min long traces measured under the same conditions as Fig. 3a and c, respectively. Events shorter than 450 ms were excluded from this analysis, yielding in total of 132 and 91 events for $Fc(MeOH)_2$ and $[Fc(CN)_6]^{3-}$, respectively. In both measurements, the histograms exhibit a sharply decreasing number of events with increasing event duration, with the majority of identifiable events having durations below 1 s.

The histograms in Fig. 3 encapsulate detailed quantitative information about the statistics of individual single-molecule trajectories. Furthermore, because mass transport is purely diffusive at the high supporting electrolyte concentrations employed here, the form of the histograms can be predicted quantitatively. This provides an unprecedentedly detailed test of electrochemical single-molecule data.

Time of first passage analysis

Within the discrete random-walk model, a single-molecule event as discussed in Fig. 3 corresponds to a molecule starting at one edge of the simulation domain and taking a number of random steps inside the device before making a final jump out either end of the simulation domain. While such an event can in principle be arbitrarily long (the molecule can hop left and right between two adjacent sites indefinitely, for example), intuition dictates that very long events should be scarce as the randomly hopping molecule is bound to hit one of the boundaries sooner or later. Conversely, very short events are expected to be common since a molecule that just entered the simulation domain need only take a few steps in the reverse direction before it exits again. This behaviour cannot be probed using measurements averaged over multiple molecules (by measuring, *e.g.*, the average current) since those signals by definition average over the contributions from multiple microscopic events. Conversely, a single event provides only very limited information. A meaningful comparison between experiment and theory can however be achieved by comparing the relative probability of the possible outcomes.

Thanks to their broad applicability in fields ranging from physics to ecology and economics, the statistics of random walks have been studied in detail. Furthermore, while numerical simulations such as those in Fig. 2 represent a useful tool for predicting the qualitative features of the data, quantitative comparison is facilitated by the use of exact analytical expressions. The event duration in our experiment and associated random-walk model corresponds to the classic problem of the so-called first-passage time for a particle undergoing a discrete random walk in a linear domain with absorbing boundaries.[18] The

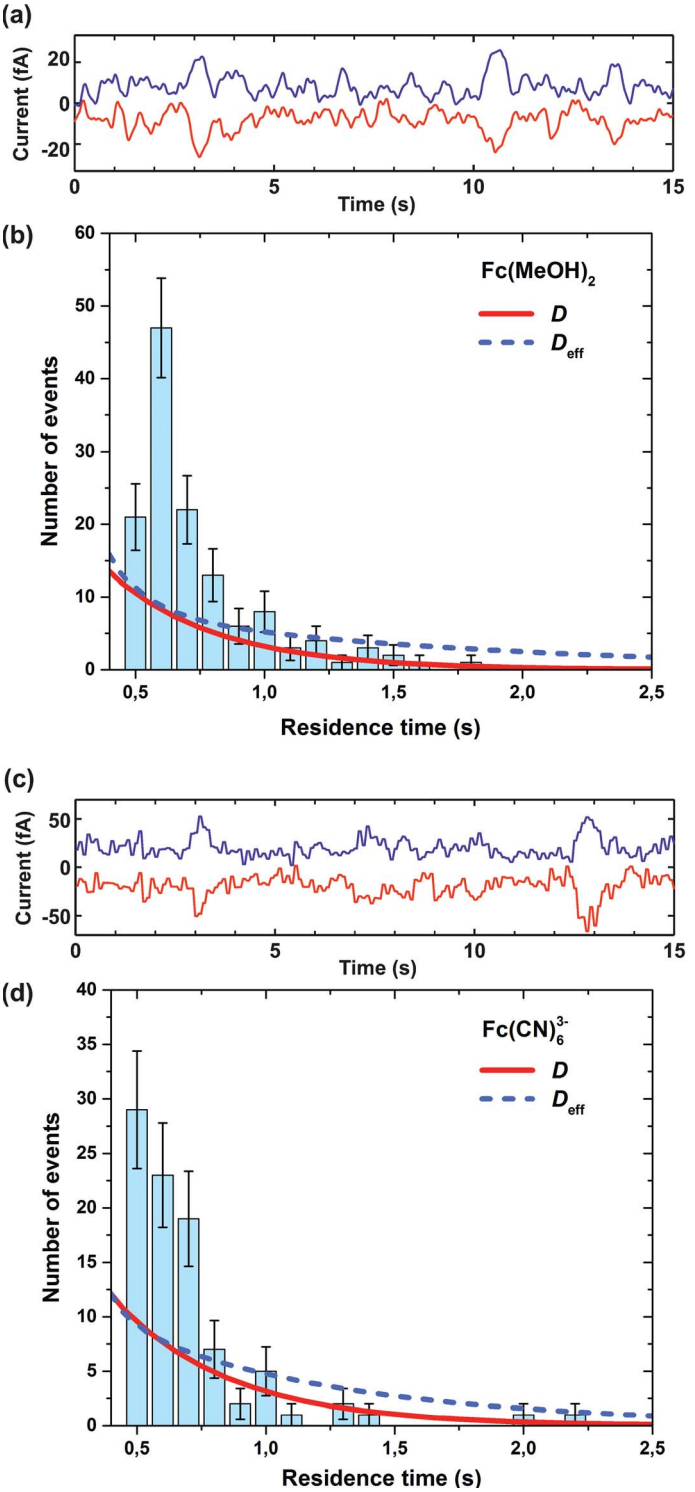

 This journal is © The Royal Society of Chemistry 2016

probability of the particle exiting after taking exactly n steps is given by the analytic expression

$$P(n) = \frac{1}{a}\sum_{\mu=1}^{a-1}\cos^{n-1}\frac{\pi\mu}{a}\sin\frac{\pi\mu}{a}\sin\frac{\pi\mu z}{a} + \frac{1}{a}\sum_{\mu=1}^{a-1}\cos^{n-1}\frac{\pi\mu}{a}\sin\frac{\pi\mu}{a}\sin\frac{\pi\mu(a-z)}{a}. \quad (1)$$

Here a is the length of the simulation domain, as above, while z is the starting position of the particle ($1 \leq z \leq a - 1$). We set $z = 1$ (or $z = a - 1$, which is equivalent from symmetry) to represent a molecule near either access hole immediately following entry of the device. The first term of the equation represents the probability that the particle exits from the same end as it entered and the second term from the opposite end. The first term diverges as $n^{-3/2}$ for small n; consequently, the most probable scenario for an event is for a molecule to enter the nanochannel and to exit again from the same end after only a few steps,[5,17] such that the residence time is very short and cannot be resolved experimentally. For large n, the distribution decays exponentially with n: in these relatively rare cases, the molecule penetrates further into the device, generating events that may be sufficiently long to be detected.

To compare theory with the experimental histogram data of Fig. 3, we renormalize eqn (1) to yield $M(t)$, the average number of events in a histogram bin of width γ and centred at time t:

$$M(t) = M_{\text{total}}\sum_{n=(t-\gamma/2)/\Delta t}^{(t+\gamma/2)/\Delta t} P(n). \quad (2)$$

Here Δt is the simulation time step as defined above and M_{total} is the total number of events that take place over the course of the measurement. The value of M_{total} is in turn obtained from $M_{\text{total}} = T\langle N\rangle/\tau_0$, where T is the total duration of the measurement, $\langle N\rangle$ is the average number of analyte molecules in the detection region, and τ_0 is the average duration of an event:

$$\tau_0 = \Delta t\sum_{n=1}^{\infty} nP(n). \quad (3)$$

These equations represent a quantitative prediction for the histogram, $M(t)$. The only inputs are experimental parameters, namely, the device length, L, the diffusion coefficient, D, the average occupancy, $\langle N\rangle$, and the duration of the measurement, T. Predictions based on the bulk diffusion coefficient ($D = 5.6 \times 10^{-10}$ m^2 s^{-1} for $Fc(MeOH)_2$ and $D = 6.0 \times 10^{-10}$ m^2 s^{-1} for $[Fe(CN)_6]^{3-}$, as determined from the diffusion-limited current at a 5 μm radius platinum ultramicroelectrode) and $\langle N\rangle$ based on the 10 pM bulk concentration are shown as red curves in Fig. 3b and d. In both cases the analytical calculation reproduces rather well the experimental data, with both the absolute number of

Fig. 3 (a, c) Representative current-time traces for 10 pM $Fc(MeOH)_2$ and $[Fe(CN)_6]^{3-}$ in 0.1 M KCl under redox cycling conditions ($E_t = 0.3$ V, $E_b = 0.2$ V, $E^{\circ\prime} = 0.25$ V and $E_t = 0.3$ V, $E_b = 0.15$ V, $E^{\circ\prime} = 0.23$ V, respectively). (b, d) Histograms (bin size $\gamma = 0.1$ s) of observed event durations and corresponding theoretical predictions for the experimental conditions of (a) and (c). Events shorter than 450 ms were excluded as they could not be resolved reliably.

events per bin and the decrease in the number of events with increasing duration being comparable between calculation and experiment apart from an excess of shorter events in the experiment.

This apparent good agreement may be fortuitous, however, as it contradicts our current understanding of microscopic diffusive dynamics in nanochannels. We have previously reported that the species studied here undergo some degree of reversible adsorption at the electrodes.[6,19,20] This is manifested by a suppression of the single-molecule current i_p such that the single-molecule current is multiplied by a factor χ_{ads} (with $0 \leq \chi_{ads} \leq 1$) compared to its ideal, diffusion-limited value,[3] $i_{p,ideal} = eD/z^2$, where $-e$ is the electron charge and z is the electrode spacing (in practice additional corrections are also included to take into account the electrode biases and the full three-dimensional geometry of the device, as per ref. 6). But reversible adsorption should also have a second consequence for mass transport, namely, that of decreasing the apparent longitudinal diffusion coefficient along the channel, D_{eff}, below its value for unhindered diffusion in bulk solution, D. These two adsorption-induced effects are directly coupled: for the simplest model in which adsorbed molecules are immobile on the electrode, $D_{eff} = \chi_{ads}D$.[6,19] We have previously observed this longitudinal behaviour in response time[21,22] and noise spectrum measurements.[17,19]

The amperometric data illustrated in Fig. 3a and c yield $\chi_{ads} = 0.3$ and 0.5 for $Fc(MeOH)_2$ and $[Fe(CN)_6]^{3-}$, respectively. Replacing D with the corresponding values of D_{eff} in eqn (1)–(3) yields the dashed green curves in Fig. 3b and d. Consistent with intuition, slower diffusion along the channel leads to a higher predicted rate of occurrence of long events for a given concentration (more precisely, the distribution gets stretched by a factor D/D_{eff} along the time axis and its amplitude is renormalized). Interestingly, however, these predictions do not agree well with the data, as significantly more long events are predicted than are observed in the experiment.

One possible interpretation of the observation that the histograms fit well with calculations using the bulk diffusion coefficient D but not with those using D_{eff} is that molecules adsorbed to the electrodes can diffuse along the channel without being slowed down substantially. In such a scenario the shuttling rate between the two electrodes is influenced by adsorption but the residence time inside the active region is not, as per the experimental findings. Surface diffusion of adsorbents has been studied in a variety of systems,[23–27] in particular using single-molecule fluorescence techniques. In some cases adsorbed molecules occupy specific binding sites but are able to move between binding sites,[24] qualitatively consistent with our observations. On the other hand, adsorption studies in nanogaps based on power spectral density (PSD) analysis[19] and transient chronoamperometric response[21,22] yield unambiguous evidence of an effective slowing down of longitudinal Brownian motion along the axis of the channel at μM and higher concentrations (five or more orders of magnitude higher than the concentration employed here). This would imply that facile hopping between binding sites is possible, but only at extremely low surface concentrations – a trend opposite to that commonly observed and described by the empirical Freundlich isotherm. Such an anomalous decrease of the surface diffusion coefficient with increasing surface concentration has been reported previously for some macromolecules and was attributed to adsorbate–adsorbate interactions.[28,29] Because the surface concentrations employed here correspond to

 This journal is © The Royal Society of Chemistry 2016

a single molecule inside the device, however, it is implausible that such an interaction mechanism applies here.

An alternate interpretation is that D_{eff} is indeed the correct diffusion coefficient, in which case an additional mechanism must be invoked to explain the missing long events when compared to the theoretical predictions. Decay of the molecules on the scale of seconds would provide such a mechanism. This can however be ruled out on the basis that the species under study are stable, the oxidized form of ferrocene derivatives for example having a lifetime on the order of an hour.[30–33] Another, more plausible hypothesis is the existence of deep trap sites[34] at which molecules can remain adsorbed for several tenths of seconds or more, causing long events to be substituted by a succession of shorter events due to repeated binding/unbinding at these sites. Consequently a reduced number of long events compensated by additional short events is expected, consistent with the experimental data. Further basis for this hypothesis comes from earlier observations in nanogap devices that adsorption becomes more pronounced at low analyte concentrations.[19,21]

Conclusion

The first-passage times of individual redox molecule trajectories were probed using electrochemical nanogap devices and their statistical distribution was compared with analytical calculations. The inability to resolve the multitude of ultra-short events was circumvented by concentrating solely on long events, this possibility of analysing a subset of the data representing one of the main strengths of single-molecule techniques.

Analysis of the distribution of the time of first passage for individual events indicates a significant suppression of the number of long events compared to that expected for a purely diffusive random walk once slowing down due to reversible adsorption is taken into account. While this would be expected if surface-bound molecules undergo facile surface diffusion, this interpretation appears incompatible with measurements at higher concentrations. Instead, the data strongly suggest that single molecules can be trapped at rare, low-energy binding sites, such that long residence times inside the detection volume are divided into shorter periods of redox cycling separated by periods of inactivity on the surface.

These measurements represent the first time that diffusive mass transport has been characterized quantitatively with single-molecule resolution using an electrochemical method.

Acknowledgements

The authors gratefully acknowledge financial support from the Netherlands Organization for Scientific Research (NWO) and the European Research Council (ERC) under project number 278801.

References

1 N. G. Walter, C. Y. Huang, A. J. Manzo and M. A. Sobhy, *Nat. Med.*, 2008, **5**, 475–489.
2 D. R. Walt, *Anal. Chem.*, 2013, **85**, 1258–1263.
3 F. R. F. Fan and A. J. Bard, *Science*, 1995, **267**, 871–874.

4 P. Sun and M. V. Mirkin, *J. Am. Chem. Soc.*, 2008, **130**, 8241–8250.
5 M. A. G. Zevenbergen, P. S. Singh, E. D. Goluch, B. L. Wolfrum and S. G. Lemay, *Nano Lett.*, 2011, **11**, 2881–2886.
6 S. Kang, A. F. Nieuwenhuis, K. Mathwig, D. Mampallil and S. G. Lemay, *ACS Nano*, 2013, **7**, 10931–10937.
7 S. G. Lemay, S. Kang, K. Mathwig and P. S. Singh, *Acc. Chem. Res.*, 2013, **46**, 369–377.
8 S. Redner, *A Guide to First-passage Processes*, Cambridge University Press, Cambridge, UK, New York, 2001.
9 P. Fauchald and T. Tveraa, *Ecology*, 2003, **84**, 282–288.
10 I. Goychuk and P. Hanggi, *Proc. Natl. Acad. Sci. U. S. A.*, 2002, **99**, 3552–3556.
11 V. J. van Hijkoop, A. J. Dammers, K. Malek and M.-O. Coppens, *J. Chem. Phys.*, 2007, **127**, 085101.
12 V. Rajani, G. Carrero, D. E. Golan, G. de Vries and C. W. Cairo, *Biophys. J.*, 2011, **100**, 1463–1472.
13 R. Mcdonald and D. Siegel, *Quarterly Journal of Economics*, 1986, **101**, 707–727.
14 A. Szabo, K. Schulten and Z. Schulten, *J. Chem. Phys.*, 1980, **72**, 4350–4357.
15 L. Hofler and R. E. Gyurcsanyi, *Anal. Chim. Acta*, 2012, **722**, 119–126.
16 Datasheet, FEMTO DDPCA-300 Variable Gain Sub Femto Ampere Current Amplifier.
17 P. S. Singh, E. Katelhon, K. Mathwig, B. Wolfrum and S. G. Lemay, *ACS Nano*, 2012, **6**, 9662–9671.
18 W. Feller, *An Introduction to Probability Theory and its Applications*, Wiley, New York, 3rd edn, 1968.
19 M. A. G. Zevenbergen, P. S. Singh, E. D. Goluch, B. L. Wolfrum and S. G. Lemay, *Anal. Chem.*, 2009, **81**, 8203–8212.
20 P. S. Singh, H. S. M. Chan, S. Kang and S. G. Lemay, *J. Am. Chem. Soc.*, 2011, **133**, 18289–18295.
21 S. Kang, K. Mathwig and S. G. Lemay, *Lab Chip*, 2012, **12**, 1262–1267.
22 K. Mathwig and S. G. Lemay, *Electrochim. Acta*, 2013, **112**, 943–949.
23 R. D. Tilton, C. R. Robertson and A. P. Gast, *J. Colloid Interface Sci.*, 1990, **137**, 192–203.
24 R. Gomer, *Rep. Prog. Phys.*, 1990, **53**, 917–1002.
25 P. R. Unwin and A. J. Bard, *J. Phys. Chem.*, 1992, **96**, 5035–5045.
26 E. G. Seebauer and C. E. Allen, *Prog. Surf. Sci.*, 1995, **49**, 265–330.
27 S. Roy, J. M. Thomas, E. A. Holmes, J. T. Kellis, A. J. Poulose, C. R. Robertson and A. P. Gast, *Anal. Chem.*, 2005, **77**, 8146–8150.
28 V. Chan, D. J. Graves, P. Fortina and S. E. McKenzie, *Langmuir*, 1997, **13**, 320–329.
29 J. Zhao and S. Granick, *J. Am. Chem. Soc.*, 2004, **126**, 6242–6243.
30 M. Avron and N. Shavit, *Anal. Biochem.*, 1963, **6**, 549–554.
31 R. Prins, A. R. Korswagen and A. G. T. G. Kortbeek, *J. Organomet. Chem.*, 1972, **39**, 335–344.
32 J. Holecek, K. Handlir, J. Klikorka and N. Dinhbang, *Collect. Czech. Chem. Commun.*, 1979, **44**, 1379–1387.
33 Z. N. Gao, X. X. Han, H. Q. Yao, B. Liang and W. Y. Liu, *Anal. Bioanal. Chem.*, 2006, **385**, 1324–1329.
34 J. Lyklema, *Fundamentals of Interface and Colloid Science*, Academic Press, San Diego, 2000.

 This journal is © The Royal Society of Chemistry 2016